Physical properties of the noncentrosymmetric superconductor Ru_7B_3

Lei Fang, Huan Yang, Xiyu Zhu, Gang Mu, Zhao-Sheng Wang, Lei Shan, Cong Ren, and Hai-Hu Wen*
National Laboratory for Superconductivity, Institute of Physics and National Laboratory for Condensed Matter Physics, Chinese Academy of Sciences, P.O. Box 603, Beijing 100190, People's Republic of China
(Received 5 November 2008; revised manuscript received 15 January 2009; published 9 April 2009)

Physical properties have been comprehensively investigated on the noncentrosymmetric superconductor Ru_7B_3 with T_C=3.3 K. It is found that the superfluid comprises a major component with a full-gap feature instead of a nodal-like pairing symmetry as revealed by specific-heat and lower-critical-field measurements. Combining with resistivity (ρ_{xx} and ρ_{xy}) and electronic band-structure calculation, the superconducting and normal-state physical parameters were determined by a self-consistent analysis. It is found that Ru_7B_3 may belong to a single band superconductor with energy gap of 0.5 meV and could be categorized into type-II superconductor with weak electron-phonon coupling. An unusual "kink" feature is clearly observed in the field induced broadening of the resistivity curves. Possible reasons are given for this unusual two-step transition.

DOI: 10.1103/PhysRevB.79.144509 PACS number(s): 74.70.Ad, 74.25.Qt, 74.25.Sv

I. INTRODUCTION

Unconventional superconductors have been extensively studied during the past decades for the underlying fundamental physics or the potential industrial applications. Some well-known examples are heavy fermion superconductors,[1] cuprates,[2] Sr_2RuO_4,[3] and the newly discovered iron arsenide.[4] In recent years superconductors lacking of lattice inversion center have received intensive attentions for the possibility of spin-triplet dominated pairing symmetry. An important example is the noncentrosymmetric superconductor $CePt_3Si$.[5] Due to the nontrivial antisymmetric spin-orbit coupling (ASOC) effect induced by the heavy platinum atom and the lacking of inversion symmetry, unconventional superconducting properties were observed; for instance the high upper critical field far beyond the Pauli-Clogston limit was found.[6] The subsequent nuclear-spin-lattice relaxation rate as well as magnetic penetration depth measurements show line nodes in the superconducting gap of $CePt_3Si$.[7,8] For a material without inversion symmetry the spin degeneracy is lifted by ASOC, under such a condition, orbital angular momentum ($\hat{L}$) and spin angular momentum ($\hat{S}$) are not good quantum numbers anymore. Thus the strict categorization of even-parity spin singlet and odd-parity spin triplet conformed to Pauli's exclusion and parity conservation is violated. Then spin-triplet component may be mixed with that of spin singlet. Up to now, several noncentrosymmetric superconductors have been reported, the development concerning such an interesting topic could be found in an overview given by Sigrist *et al.*[9] However strong electronic correlation in some materials complicates the studies on ASOC effect, such as the heavy fermion characteristics of $CePt_3Si$. Recently the pairing symmetry of Li_2Pt_3B was proved to be consistent with the picture of line nodes,[10,11] such a material is not strongly correlated and could be regarded as an appropriate example for investigating the ASOC effect. For more comprehension on ASOC, any efforts to study on the properties of noncentrosymmetric superconductors are worthwhile, especially in the system with small electron correlation effect.

In the present paper we focus on the ruthenium-based superconductor Ru_7B_3 with T_C equal to 3.3 K. An important characteristic of this superconductor is the lacking of inversion center, which was pointed out by Morniroli[12] based on the structural analysis. Thus a detailed investigation on the paring symmetry of this compound is very attractive. To our best knowledge, the physical properties have not been investigated comprehensively in this material. It was mentioned only by Matthias in the early 1960s[13] that the material Ru_7B_3 had a T_C of about 2.58 K. So physical properties of Ru_7B_3 are deserved to be studied with the purpose to know that whether the noncentrosymmetry could lead to some unusual properties. Specific-heat and lower-critical-field measurements reveal that Ru_7B_3 could be described as an *s*-wave-dominated superconductor. While an unusual "kink" structure was observed in the resistive transitions under magnetic fields.

The paper is organized as follows. Section II describes the sample preparation and the experimental details. Then in Sec. III we provide the structure illustration and the measurements of ac magnetization and many transport properties, including resistivity, magnetoresistance, and Hall coefficient. Section IV presents the specific-heat and lower-critical-field measurements. In the following Sec. V, a full potential electronic band-structure calculation is presented. Finally, in Sec. VI, parameters of the normal and superconducting states are obtained and shown to be in good self-consistency.

II. EXPERIMENT

Polycrystalline sample Ru_7B_3 was synthesized by conventional solid-state sintering process. Stoichiometric ruthenium powder (purity 99.9%) and boron powder (purity 99.95%) were mixed together and grounded thoroughly, then the mixture was pressed into pellet with a pressure 10 MPa. The pellet was wrapped with tantalum foil and sealed into an evacuated silicon tube. A gas mixture of 95% high-purity Ar with 5% H_2 was used as the protected atmosphere. The tube was warmed up to 1000 °C in a muffle furnace with a rate of 100 °C/h and sintered for 100 h for composition homogeneity, then the furnace was cooled down to room temperature. The ingot was ceramiclike with a silver gray color. It was observed that the sample quality was stable and insen-

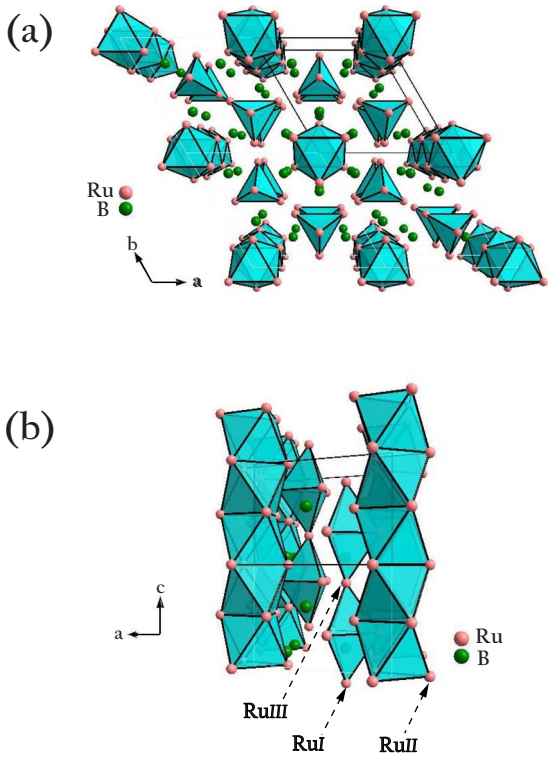

FIG. 1. (Color online) (a) Top view (*ab* projection) of the Ru_7B_3 structure. The skeleton consists of metal tetrahedra and metal octahedra and interstitial boron anions. From such a projection, the lattice with hexagonal rotation symmetry is obvious. (b) The *ac* projection of the lattice, "two chains" are built up by ruthenium ions at different coordinations.

sitive to humidity or oxygen. No obvious change of the superconducting transition was found after the sample had been kept in air for about one year. X-ray diffraction (XRD) pattern measurement was performed at room temperature employing an M18AHF x-ray diffractometer (MAC Science). Cu $K\alpha$ was used as the radiation target. Crystallographic orientation and index were determined by POWDER-X,[14] a software for processing x-ray diffraction data. The ac susceptibility were measured based on an Oxford cryogenic system (Maglab-Exa-12). The resistivity and specific heat were measured on the Quantum Design instrument physical properties measurement system (PPMS) with temperature down to 1.8 K and the PPMS-based dilution refrigerator (DR) down to 50 mK. The temperatures of both systems have been well calibrated, showing consistency with an error below 2% in the temperature range from 1.8 to 10 K. The lower-critical-field measurement was based on a two-dimensional electron-gas (2DEG) micro-Hall probe with an active area of 10×10 μm^2. All $M(H)$ curves were taken in the zero-field-cooled mode with initial temperature up to 6 K. A low-field sweep rate of 60 Oe/min was selected to measure isothermal magnetization curves. Self-consistent band-structure calculations were carried out using the linear-muffin-tin-orbital (LMTO) method on full potential plane-wave representation (FP-LMTO-PLW).[15]

III. STRUCTURE ILLUSTRATION AND TRANSPORT PROPERTIES

The crystal structure of Ru_7B_3 was determined by Aronsson[16] in the late 1950s. It was found that the lattice is hexagonal with a space group $P6_3mc$. There are 20 atoms in one unit cell with effective coordinate $Ru_I(6c)$, $Ru_{II}(6c)$, $Ru_{III}(2b)$, and $B(6c)$, respectively. Thus two formula units exist in one unit cell. In that paper the author gave a relative comprehensive description to the lattice structure of Ru_7B_3; however, thanks to the complex structure of transition metal boride, a more detailed illustration should be added as a supplement for better comprehension on its properties. As to space group $P6_3mc$, a distinct characterization of the crystal lattice is without inversion symmetry. For example, the center of Boron atoms' sublattice dislocates the counterpart of Ruthenium atoms along *c* axis; thus the inversion symmetry is broken along such direction. For more clear understanding on the crystal lattice, we illustrate the structure along two type projections in Fig. 1. Figure 1(a) shows the *ab* projection of Ru_7B_3 structure. It is found that the skeleton consists of metal tetrahedra and metal octahedra and interstitial boron anions. From such a projection, the lattice with hexagonal rotation symmetry is obvious. Figure 1(b) is the ac projection illustration. A very interesting phenomenon is that two "chains" are built up by ruthenium ions at different coordinations. The metal octahedra at each corner of the lattice is built up by $Ru_{II}(6c)$, those octahedra share face along *c* axis and thus a zigzag chain is formed as shown in Fig. 1(b). The rest $Ru_I(6c)$ and $Ru_{III}(2b)$ form two tetrahedra in one unit cell at different (x,y) positions, along *c* direction two tetrahedra [at the same (x,y) positions] share face and then forming a hexahedra, each hexahedra is connected by $Ru_{III}(2b)$ and thus another type of row is formed. The special structure configuration might play an important role in transport properties; also the environment of Ruthenium ions (including

TABLE I. Structure parameters of Ru_7B_3 (Ref. 16).

Atom	Cite	*x*	*z*	Number[a]	*l* [b] (Å)
Ru_I	6*c*	0.4563	0.318	4	2.15, 2.15, 2.66, 2.66
Ru_{II}	6*c*	0.1219	0	4	2.15, 2.16, 2.16, 2.86
Ru_{III}	2*b*	1/3	0.818	3	2.20, 2.20, 2.20
B	6*c*	0.187	0.582		

[a]Number of nearest Boron for different cites of ruthenium.
[b]Interatomic distance between boron and ruthenium ions.

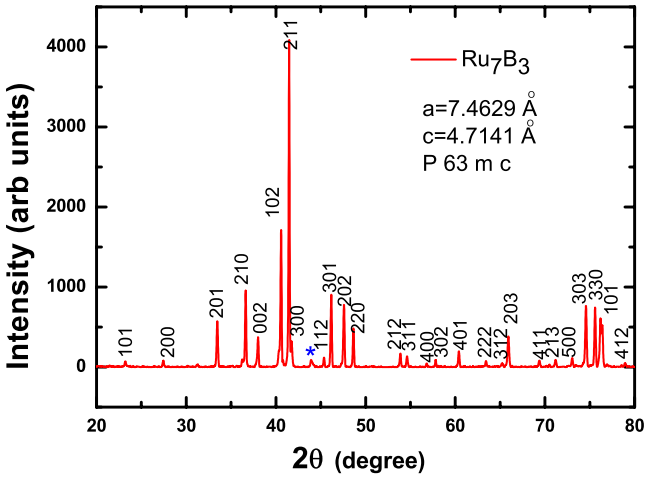

FIG. 2. (Color online) X-ray diffraction pattern of Ru_7B_3. Most of the diffraction peaks are indexed except for one minor peak possibly coming from unreacted boron; the purity is estimated to be about 95%. The asterisk marks the peak from impurity phase.

the interatomic distance and the number of the nearest boron ions) is very important. Detailed parameters are included in Table I as shown below.

Figure 2 shows the XRD pattern of the sample Ru_7B_3, which can be indexed in a hexagonal symmetry with $a=b=7.4629$ Å and $c=4.7141$ Å. The indexed indices slightly deviate from the reported parameters $a=b=7.467$ Å and $c=4.713$ Å. It is clearly found that most diffraction peaks are indexed except for one minor peak possibly coming from unreacted boron. From the quality of XRD data, it is estimated that the purity of Ru_7B_3 we synthesized is about 95%. In the following specific-heat measurement, it will be shown that the superconducting component exceeds about 90%, indicating a good sample quality.

Figure 3 presents the ac susceptibility measurement under different magnetic fields. It is found that a sharp diamagnetic

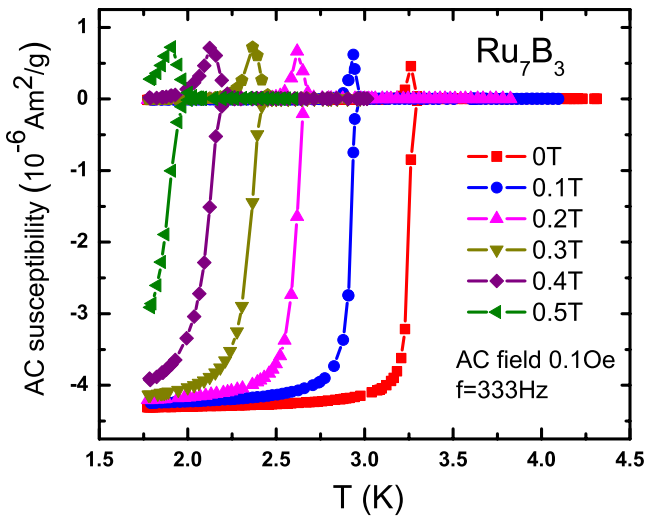

FIG. 3. (Color online) ac susceptibility of Ru_7B_3, a sharp superconducting transition happens at 3.3 K under zero field; a narrow transition width less than 0.3 K indicates the good superconducting quality.

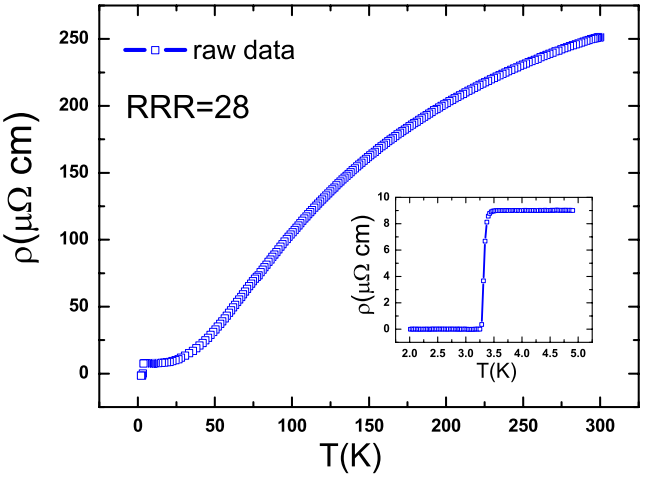

FIG. 4. (Color online) Resistivity of Ru_7B_3 under zero field is measured from 2 K to room temperatures. A relative high RRR indicates the high quality of the samples. The inset shows the enlargement of superconducting transition; the transition width is less than 0.3 K.

transition happens at 3.3 K and the diamagnetic value approaches a constant at 3 K. The transition width of only 0.3 K was observed, indicating good quality of the sample. By applying magnetic fields, the transition curve moves parallel to low temperatures. For estimating the upper critical field, we take 5% of saturation magnetization value as the criterion and will show the results in Fig. 6.

Figure 4 shows the resistivity data from 2 K to room temperatures. The curve shows a good metallic behavior with a residual resistivity (ρ_0) 9 $\mu\Omega\cdot$cm. Such a high conductivity is the common feature of transition metal boride. It is found that the residual resistivity ratio (RRR) is 28. The relative high RRR in polycrystalline sample indicates the high quality of our sample. The inset of Fig. 4 shows the enlargement of superconducting transition. One can see that the resistivity drops sharply to zero at 3.3 K. Thus the resistivity data and ac susceptibility give a self-consistent $T_C=3.3$ K for Ru_7B_3, which is slightly higher than the value of $T_C\approx 2.58$ K as preliminary mentioned by Matthias.[13]

Figure 5 shows the field broadening of the resistivity curve on the polycrystalline sample Ru_7B_3 down to 100 mK. When a magnetic field is applied, the onset part of the transition is rounded which might be induced by the critical fluctuation in superconductors. While increasing the magnetic fields to 0.6 T, the rounded part of transition evolves into a kink structure as shown clearly in Fig. 5. It seems that the kinks break the superconducting transition curves into two parts: The lower part moves quickly to low temperatures showing a strong dependence of magnetic fields, while the upper parts show a much weaker depression of magnetic fields. It is observed that the zero resistivity point approaches zero temperature when sample is bearing 1.1 T magnetic field, while superconductivity (onset transition point) is depressed completely at about 5 T. It is thus very interesting to note that the determined upper critical field strongly depends on the selected criterion of resistivity.

As shown in Fig. 6, using the criterion of 99% ρ_n and zero, we obtained two distinct $H_{C2}(0)$ curves with a ratio of

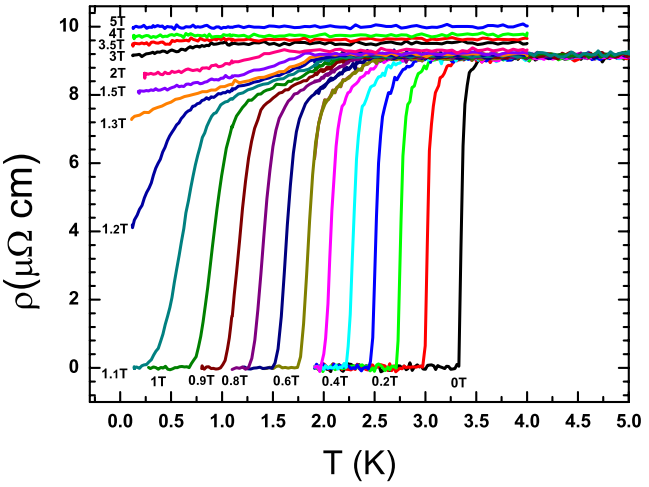

FIG. 5. (Color online) Field-broadening superconducting transition curves of Ru_7B_3 from 0.1 to 4 K; a clear "kink" feature appears as the field exceeds 0.6 T. The superconducting transition is completely removed by applying a magnetic field of 5 T. Distinct magnetoresistance was observed in the normal state.

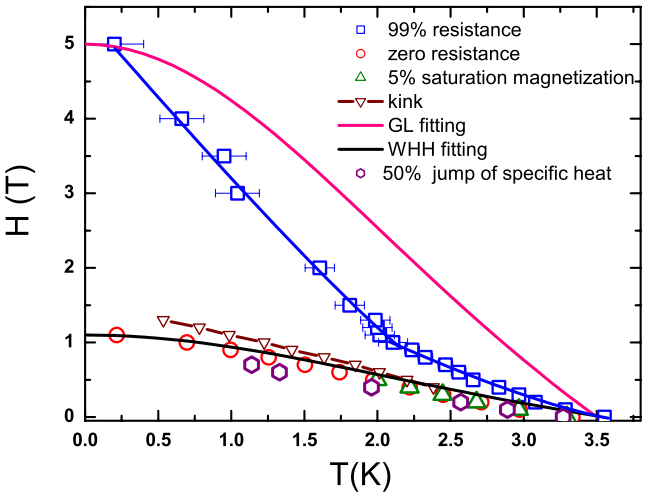

FIG. 6. (Color online) Phase diagram of Ru_7B_3; a nontrivial flux flow appears in the area determined by using the criteria of 99%ρ_n and zero resistance. We also adopted the 5% saturated magnetization signal from ac susceptibility and the position at the half height of the specific-heat anomaly as criteria to estimate the intrinsic value of $H_{C2}(0)$. It is shown that except for that with the criterion of 99% ρ_n, the values with other three methods overlap each other. For the lower transition, the $H_{C2}(0)$ was found to be about 1.1 T. It is found that the calculated result of H_{C2} using the Werthamer-Helfand-Hohenberg (WHH) formula fits experimental data of the second transition very well. The $H_{C2}(T)$ data determined with the criterion of 99% ρ_n cannot be described by either the Ginzburg-Landau or the WHH theory.

about 5. Several reasons could be attributed to the significant difference of $H_{C2}(0)$ determined with different criterion. The first one concerns the superconducting fluctuation.[17] However taking account of the very low T_C and relatively large H_C (see below), the superconducting fluctuation is believed to be weak since the ratio between the condensation energy $H_C^2/8\pi\xi^3$ and k_BT_C is rather large. A second concern about the kink feature observed in resistive transition curves under moderate fields would be the inhomogeneity of superconductivity. If there are some impurity phases, the measurements on the magnetic and the specific heat would see broad transitions. However the sharp transitions in resistivity, magnetization, and specific heat at zero field seem to exclude this possibility obviously. Also the relatively clean XRD data seem to be inconsistent with this argument. The third interpretation would rely on the granular superconductivity, especially when the anisotropy is large. For a granular superconductor, there are superconducting weak links between these grains. At zero or a weak field, the superconducting current can flow through these weak links and a sharp transition can be observed; while when the magnetic field is high, the weak links are truncated, in this case a finite resistivity will show up but the onset transition point corresponds to the $H_{C2}(0)$ of the grains. The large H_{C2} anisotropy in polycrystalline sample could be another possibility.[18,19] In the polycrystalline sample, the grains are oriented randomly. If the H_{C2} is anisotropic, the superconductivity will be lost first in those grains with low H_{C2} values, and then the ones with higher H_{C2} values. A similar phenomenon has been observed in polycrystalline MgB_2 and was explained by H_{C2} anisotropy and current percolation. In the following description of specific-heat measurement, the jump in specific heat significantly broadens with fields, which could be the further hint for H_{C2} anisotropy. However in the polycrystalline samples of $Mg_{10}Ir_{19}B_6$,[20,21] this phenomenon has not been observed. One more possibility, which may be a very attractive one, is that there might be two components which correspond to the spin singlet and triplet pairing in the superconductor. The spin singlet one has a large ratio as evidenced by the specific heat and magnetic signal, while the triplet one takes only a small ratio and thus superfluid associated with this component is diluted but the upper critical field is high. However no detection for this diluted component from susceptibility and specific-heat measurements could be against such a point of view. Nonetheless, considering the discrepancy among experimental results, further efforts are strongly demanded to clarify this issue. If In Fig. 6 we plot the phase diagram of Ru_7B_3, the criteria are taken as stated below, for zero resistivity and 99% ρ_n, for 5% saturated signal of the magnetization and the half position of specific-heat anomaly for thermodynamic measurement. The derived value of dH_{C2}/dT equals to −0.43 T/K or −0.277 T/K for the criteria of 99% ρ_n and zero resistance, respectively. It is found that except for the data with the criteria of 99% ρ_n, the other three sets of $H_{C2}(0)$ determined with different criterion overlap each other. The specific-heat measurements provide values of $H_{C2}(0)=1.1$ T and $dH_{C2}/dT=-0.277$ T/K near T_C. We also try to use the Ginzburg-Landau formula to fit the data determined by adopting the criterion of 99% ρ_n,

$$H_{C2}(T) = H_{C2}(0)\frac{1-t^2}{1+t^2}, \tag{1}$$

where t is the normalized temperature T/T_C. It is found that the fitting curve strongly deviates from the 99% ρ_n points as shown in Fig. 6, indicating that the H_{C2} determined by the

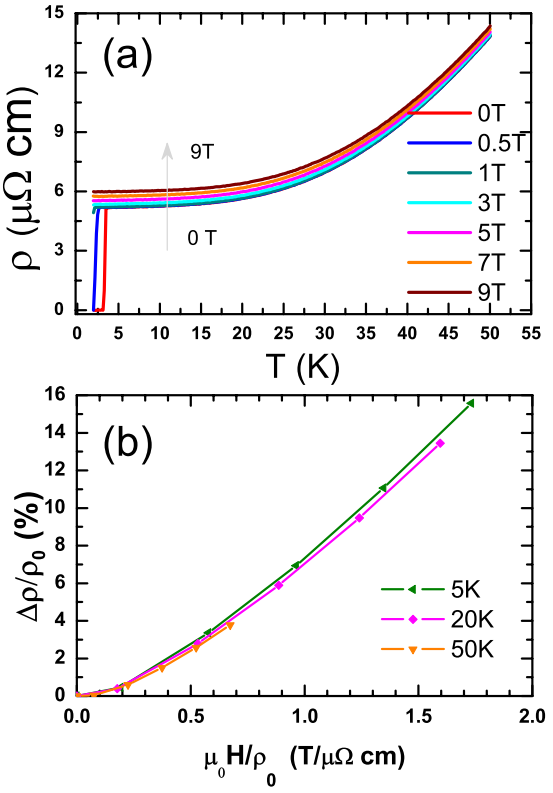

FIG. 7. (Color online) (a) Temperature dependence of resistivity of Ru_7B_3 under magnetic fields ranging from 0 to 9 T. (b) The derived magnetoresistance $\Delta\rho/\rho_0$ is 16% at 5 K at 9 T. It is shown that the scaling of Kohler's law is slightly violated. The violation may be attributed to the band splitting by ASOC instead of multiband effect.

very onset of the resistivity drop cannot be described by the GL theory.

Another distinct characteristic of Fig. 5 is the field-induced magnetoresistance (MR). Typically magnetoresistance is used to investigate the electronic scattering process and provide useful information on Fermi surface (FS) topology or the electronic band structure. Thus detailed studies are needed. In Fig. 7 we present the temperature dependence of resistivity under magnetic fields ranging from 0 to 9 T. It is found that the magnetoresistance is about 16% $[(\rho_{9\,\mathrm{T}}-\rho_{0\,\mathrm{T}})/\rho_{0\,\mathrm{T}}]$ at 5 K, which is one order of magnitude larger than the ratio of recently discovered iron arsenide $LaFeAsO_{1-x}F_x$.[22] The latter was regarded as a superconductor with multiple bands. A simple verification for the possibility of multiband effect is to scale the data $\rho(T)$ measured under different fields based on Kohler's rule, which was written in the way as $\Delta\rho/\rho_0=F(H/\rho_0)$, where F is a unknown function depending on the nature of the electronic system. For a single-band metal with symmetric Fermi surface, the Kohler's law should be satisfied. It is shown in Fig. 7(b) that the Kohler's rule is only slightly violated in Ru_7B_3, unlike the case in multiband systems such as MgB_2 (Ref. 23) and $LaFeAsO_{1-x}F_x$. The further specific-heat and lower-critical-field measurements provide the similar conclusion. However we believe that the slightly violation of Kohler's rule could be induced by the noncentrosymmetric structure

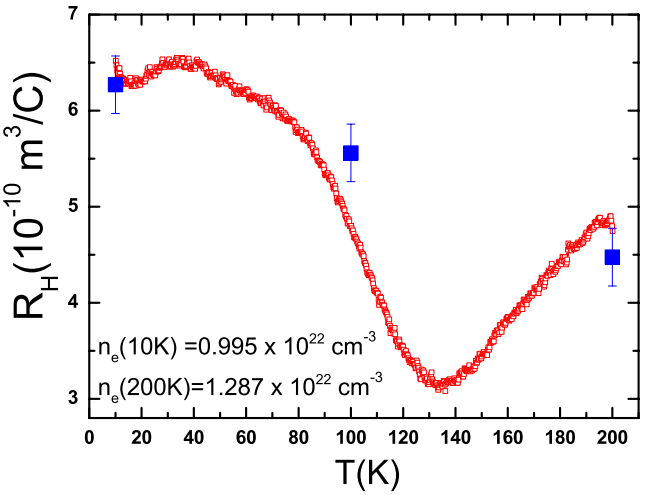

FIG. 8. (Color online) Hall coefficient of Ru_7B_3 measured by sweeping temperature under fixed fields (dense data) and that determined by sweeping the field from −9 to 9 T at three fixed temperatures (filled squares with error bars). It is found that the holelike charge carriers dominate the conduction from low temperature to 200 K, with the carrier density of about $1\times10^{22}/\mathrm{cm}^{-3}$.

of Ru_7B_3; due to the ASOC, the degenerate spin-up and spin-down bands are spilt.

Hall-coefficient (R_H) measurement was done by sweeping temperature at magnetic field 9 T and reversing field (−9 T). For avoiding the possible temperature hysteresis, increasing temperature mode with a moderate rate 1 K/min was adopted for both positive and negative fields. The Hall coefficient is shown in Fig. 8. It is found that the charge carrier of Ru_7B_3 is dominated by holelike carriers with R_H $3\sim6\times10^{-10}$ m^3/C from 2 to 200 K. For verifying the R_H in the way mentioned above, we also determine the values by sweeping magnetic field at three temperature points 2, 100, and 200 K. The low temperature R_H is consistent with the value from sweeping temperature, while slight discrepancy exists at high temperatures. The charge-carrier density calculated by $n=1/(R_He)$ is about $1\times10^{22}/\mathrm{cm}^3$, which is two orders of magnitude larger than that in superconductors with low carrier density, for example, cuprates[24] and hole-doped iron arsenide $(La_{1-x}Sr_x)FeAsO$.[25] We also notice the nonlinear temperature dependence of $R_H(T)$. However, as shown in Fig. 8, the relative change of R_H from 2 to 200 K is small. Moreover, it is known that the Hall effect is very sensitive to the temperature-dependent scattering rate, local Fermi velocity, and complex FS topology.[26] Thus considering the nature of a polycrystalline sample, it is difficult to conclude about the intrinsic properties from the Hall coefficient.

IV. SPECIFIC-HEAT AND LOWER-CRITICAL-FIELD MEASUREMENT

A. Specific heat

Figure 9 shows the raw data of specific heat under different magnetic fields from zero to 3 T. With increasing field the specific-heat anomaly near T_C moves quickly to low temperatures, leaving a background connected well with that

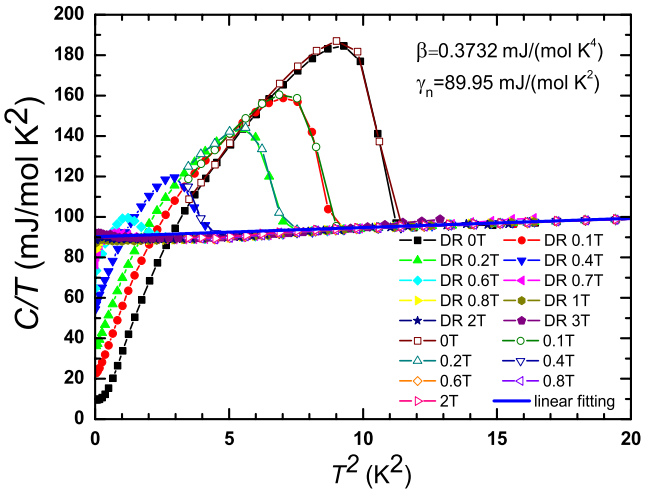

FIG. 9. (Color online) Raw data of specific heat plotted as C/T vs T^2. All filled symbols represent the data taken with the DR based on the PPMS at various magnetic fields. The open squares show the data taken with the PPMS at different fields. The thick solid line represents the normal-state specific heat which contains both the phonon γ_{ph} and the electronic contributions.

above T_C. Regarding the relatively low T_C of the present sample, the normal-state specific heat could be extracted easily with the simple relation $C/T=\gamma_n+\beta T^2$, where γ_n is the normal-state specific-heat coefficient and β corresponds to phonon contribution. By fitting to the data in the normal state, it is found that $\beta=0.3732$ mJ/mol K^4 and $\gamma_n=89.95$ mJ/mol K^2. By extrapolating the low-temperature data of zero field down to zero K, one obtains a residual value $\gamma_0\approx 9.8$ mJ/mol K^2, which suggests the existence of about 10% nonsuperconducting fraction. This nonsuperconducting fraction could partly come from unreacted boron as inferred from analysis on the XRD data. Thus the normal-state Sommerfeld constant could be determined from the relation $\gamma_e=\gamma_n-\gamma_0$, yielding 80.15 mJ/mol K^2. Using the relation $\Theta_D=(12\pi^4 k_B N_A Z/5\beta)^{1/3}$, where $N_A=6.02\times 10^{23}$ is the Avogadro constant and Z=20 is the number of atoms in one unit cell, we get the Debye temperature $\Theta_D=470.18$ K. It is noticed that the value of γ_n determined in our measurement is higher than that of $Mg_{10}Ir_{19}B_6$ (Ref. 21) and Li_2Pt_3B,[27] indicating the higher density of state in Ru_7B_3. Furthermore we could estimate the electron-phonon coupling constant $\lambda_{e\text{-Ph}}$ via McMillan equation[28]

$$T_C=\frac{\Theta_D}{1.45}exp\left[-\frac{1.04(1+\lambda_{e\text{-Ph}})}{\lambda_{e\text{-Ph}}-\mu^*(1+0.62\lambda_{e\text{-Ph}})}\right], \qquad (2)$$

where μ^* is the Coulomb pseudopotential taking about 0.11. Using $\Theta_D=470.175$ K and $T_C=3.3$ K, we obtain $\lambda_{e\text{-Ph}}=0.48$. This value indicates that Ru_7B_3 belongs to a weak-coupling superconductor.

For noncentrosymmetric superconductors, pairing symmetry could be achieved due to the mixing of spin singlet and spin triplet. Specific heat is a useful tool to investigate the low-energy excitation of quasiparticles in a material. Therefore, in Fig. 10(a), we present the temperature dependence of γ_e under magnetic fields up to 3 T by subtracting

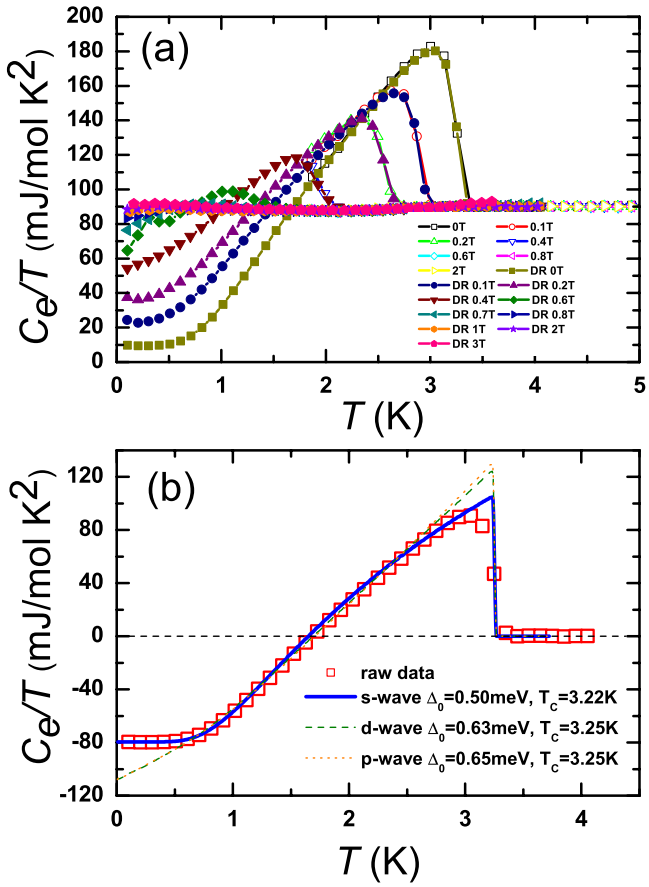

FIG. 10. (Color online) (a) Temperature dependence of γ_e for magnetic fields up to 3 T; (b) Temperature dependence of γ_{ne}-γ_e at zero field. The blue solid, green dashed, and orange dotted lines are theoretical curves calculated based on BCS model with a gap of *s* wave, *d* wave, and *p* wave, respectively.

the phonon contribution. For the convenience of theoretical analysis, we further subtract γ_n of zero-field data as shown in Fig. 10(b). Thus the weak-coupling Bardeen-Cooper-Schrieffer (BCS) formula could be used,

$$\gamma_e(T)=\frac{4N(0)}{k_B T^3}\int_0^{\hbar\varpi_D}\int_0^{2\pi}\frac{e^{\xi/k_BT}}{(1+e^{\xi/k_BT})^2}\times\left[\varepsilon^2+\Delta^2(\theta,T)-\frac{T}{2}\frac{d\Delta^2(\theta,T)}{dT}\right]d\theta d\varepsilon, \qquad (3)$$

where $\zeta=\sqrt{\varepsilon^2+\Delta^2(T,\theta)}$. In obtaining the theoretical fit we take the implicit relation $\Delta_0(T)$ derived from the weak-coupling BCS theory for superconductors with different pairing symmetries: $\Delta(T,\theta)=\Delta_0(T)$ for *s* wave, $\Delta(T,\theta)=\Delta_0(T)\cos 2\theta$ for *d* wave, and $\Delta(T,\theta)=\Delta_0(T)\cos\theta$ for *p* wave, respectively. The theoretical curve of *s* wave fits the experimental data very well, leading to an isotropic gap value $\Delta_0=0.5$ meV and $T_C=3.22$ K. The ratio $\Delta_0/k_BT_C=1.80$ obtained here is quite close to the prediction for the weak-coupling limit ($\Delta_0/k_BT_C=1.76$). In addition, the specific-heat anomaly at T_C is $\Delta C_e/\gamma_n T|_{T_C}\approx 1.31$ being very close to the theoretical value 1.43 predicted for the case of weak coupling. Therefore from the results of specific-heat

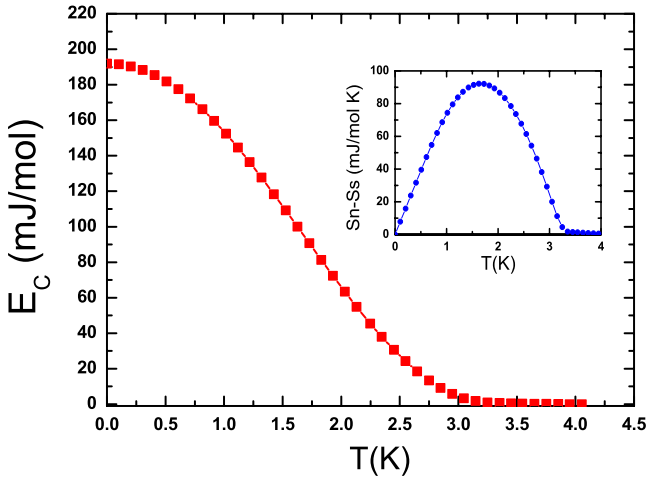

FIG. 11. (Color online) Superconducting condensation energy of Ru_7B_3 calculated by using specific-heat data. The inset shows the entropy difference between the normal and superconducting states.

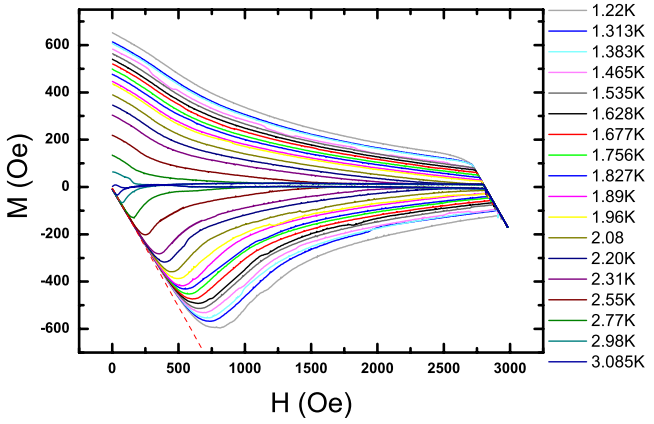

FIG. 12. (Color online) The raw data of $M(H)$ curves at different temperatures. It is found that the $M(H)$ curves measured at different temperatures all exhibit a common linear dependence on the magnetic field, which gives the Meissner shielding line, as marked by the red dashed line.

measurement, we conclude that Ru_7B_3 is a superconductor possessing a major component of superfluid with an isotropic gap, which is obviously contrast with other noncentrosymmetric superconductors such as Li_2Pt_3B and $CePt_3Si$ with anisotropic gaps based on the measurement of specific heat.[27,29]

Condensation energy (E_C) is an important parameter for a superconductor; thus in the following we calculate E_C with the specific-heat data. The entropy difference between normal state and superconducting state could be obtained by $S_n - S_s = \int_0^T (\gamma_n - \gamma_e) dT'$, and E_C is determined through $E_c = \int_T^{4K} (S_n - S_s) dT'$. The resulted temperature dependence of E_C is shown in Fig. 11. The inset shows the entropy difference between normal state and superconducting state. E_C is about 192 mJ/mol at 0 K. Alternatively, E_C could be calculated by the following equation:

$$E_c = \alpha N(E_F)\Delta_0^2/2 = \alpha \frac{3}{4\pi^2}\frac{1}{k_B^2}\gamma_n \Delta_0^2. \quad (4)$$

For a BCS s-wave superconductor, α takes unity, taking $\gamma_n = 80.15$ mJ/mol·K^2 and $\Delta_0 = 0.5$ meV, we obtain a value of 205 mJ/mol for the condensation energy, which is close to 192 mJ/mol obtained above. The consistency between the values determined using two different methods reversely verifies the validity of γ_n and Δ_0 determined through our experiment. From condensation energy, the thermodynamic critical field $\mu_0 H_C(0)$ could be calculated via the relation $\mu_0 H_C^2(0)/2 = F_N - F_S = \int\int (\gamma_n - \gamma_e) dT$, yielding $H_C(0) = 612$ Oe. For a comparison, $H_C(0)$ of another noncentrosymmetric superconductor $Mg_{10}Ir_{19}B_6$ is about 300 Oe.[20]

B. Lower-critical-field measurement

Lower critical field (H_{C1}) is an important parameter for a superconductor. According to the Ginzburg-Landau theory, H_{C1} reflects the superfluid density ρ_s since H_{C1} is related to London penetration depth λ as $H_{C1} \sim 1/\lambda^2$. Moreover, the temperature dependence of H_{C1}, especially the low-temperature feature, is often used to investigate the superconducting pairing symmetry and multigap effect. In this section we use a 2DEG micro-Hall probe to measure the local magnetization loops of Ru_7B_3. In order to precisely determine the low critical field, we used a low-field sweep rate of 60 Oe/min to measure the isothermal magnetization curves.

Figure 12 shows the initial part of the isothermal $M(H)$ curves over the temperature range from 1.22 to 3.2 K. It is found that the low-field parts of these $M(H)$ curves overlap almost on one common line (as shown by the red dashed line), which is attributed to Meissner effect and called as Meissner line. Thus H_{C1} could be determined as the deviating point between $M(H)$ curve and the Meissner line with the same criterion for all curves. The resulted temperature dependence of H_{C1}(T) [normalized to $H_{C1}(0)$] is shown in Fig. 13. The inset of Fig. 13 shows the criterion for determining the value of H_{C1} at 1.4 K. The error bar is about 10 Oe.

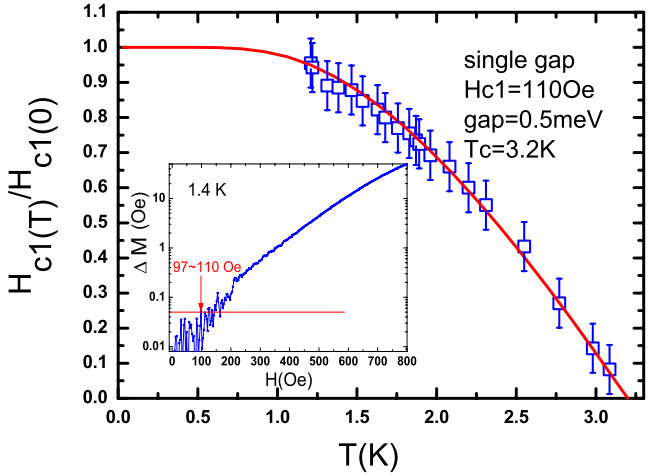

FIG. 13. (Color online) The extracted H_{C1} as a function of temperature, isotropic s wave with gap value 0.5 meV could give a good fitting to the experimental data. The inset shows the way we determine the H_{C1} at 1.4 K.

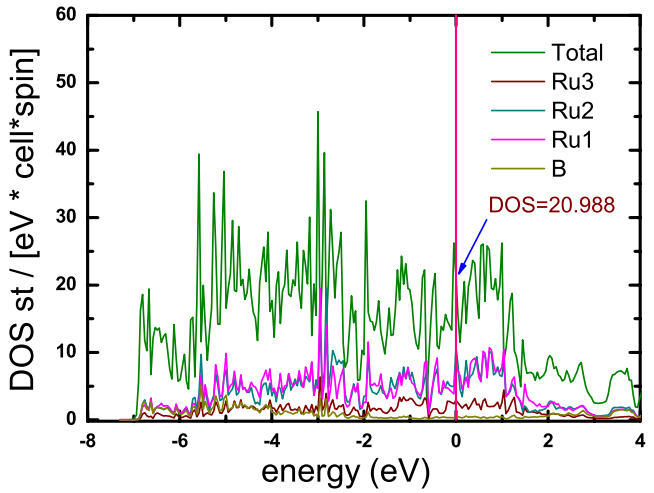

FIG. 14. (Color online) Density of states of Ru_7B_3 calculated by using the full potential PLW-LMTO method. The DOS at chemical potential is about 20.988 state/(eV cell spin). It is shown that electronic structure is dominated by ruthenium 4*d* band; the boron 2*p* orbital contributes very little to the total DOS.

According to BCS theory for clean superconductors, the normalized $H_{C1}(T)/H_{C1}(0)$ is expressed as follows:[30]

$$\frac{H_{C1}(T)}{H_{C1}(0)} \propto \frac{\lambda^2(0)}{\lambda^2(T)} = 1 - 2\int_{\Delta(T)}^{\infty} \left[-\frac{\partial f(E)}{\partial(E)}\right] D(E)d(E), \quad (5)$$

where $\Delta(T)$ is the BCS superconducting energy gap, $f(E) = 1/[\exp(-E/k_BT)+1]$ is the Fermi distribution function, and $D(E)=E/[E^2-\Delta^2(T)]^{1/2}$ is the quasiparticle density of states. We use above equation to fit the experimental data with $H_{C1}(0)$ and $\Delta(0)$ as the fitting parameters. It is found that the model of a single *s*-wave pairing gap could give an appropriate fit with fitting values $H_{C1}(0)=110$ Oe and $\Delta(0)=0.5$ meV, the latter is consistent with that of specific-heat measurement. Thus the good consistence indicates the reliability of results determined by H_{C1} measurement, although the experimental data in lower temperature region (below 1.2 K) is absent. Nevertheless, the result determined by lower-critical-field measurement afford another important evidence beyond specific heat and the common conclusion is that the pairing symmetry of Ru_7B_3 is dominated by an isotropic *s*-wave gap.

V. ELECTRONIC BAND-STRUCTURE CALCULATION

In this section we present the results of density of states (DOS) and band dispersion based on the calculations using the full potential linear-muffin-tin-orbital program LMTART by Savrasov.[15,31] Full potential approximation PLW is selected and believed to give the adequate accuracy. Figure 14 is the DOS calculated for Ru_7B_3. The total DOS curve has numerous singularities; the feature is very similar to that of $Mg_{10}Ir_{19}B_{16}$.[32] In that paper the author attributed the characterization as large numbers of atom in the unit cell and various interatomic distances. In Ru_7B_3 only 20 atoms exist in one unit cell; thus the numerous van Hove singularities could stem from the various interatomic distances complicated by the lacking of an inversion center. Another feature is that electronic structure is dominated by Ruthenium 4*d* states, while the boron 2*p* orbital contributes little. It is reasonable to understand from structure aspect that the lattice of Ru_7B_3 is mainly constructed by metal tetrahedra and metal octahedra or "chains" along *c* direction; thus charge carries naturally favor those special channels in a crystal lattice. The total DOS at chemical potential for Ru_7B_3 is 20.988 state/eV per formula unit. For checking the calculated DOS at chemical potential, we could simply estimate the DOS from γ_n in the framework of free-electron gas as

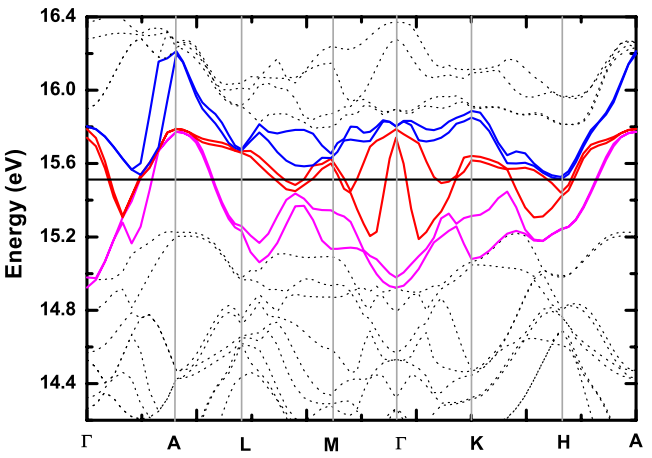

FIG. 15. (Color online) Band dispersion curves of noncentrosymmetric materials Ru_7B_3; the bands are doubly bound due to the ASOC induced spin-up and spin-down splitting.

$$N(0) = \left(\frac{2\pi^2 k_B^2}{3}\right)^{-1} \cdot \gamma_n, \quad (6)$$

where γ_n is selected as 80.15 mJ/mol K^2, $k_B=1.380\,658 \times 10^{-23}$ J/K is the Boltzmann constant, and $N(0)$ represents the density of states. The obtained $N(0)$ is about 17 state/cell per formula, which is close to the calculated value 20.988. Figure 15 is the band dispersion curves near Fermi energy. A distinct feature is that the all bands are doubly accompanied. This feature is attributed to the antisymmetric spin-orbit coupling effect; thus the degeneracy of spin-up and spin-down is lifted. It is noticed that at some *k* points with high symmetry, orbital splitting instead of degeneracy also exists, which could come from problems such as inadequate optimized parameters at initialization during computation. Nevertheless, it is believed that such stigma cannot affect the main results of the present work.

VI. DISCUSSION ON ASOC EFFECT AND SELF-CONSISTENCY AMONG SUPERCONDUCTING PARAMETERS

In this paragraph we first give a brief discussion on the possibility of exotic properties due to ASOC in Ru_7B_3. Generally, two criteria for superconductivity in the framework of noncentrosymmetry have been established. The first one is the Pauli-Clogston limiting field,[6] which could be expressed as $H_p(0)=\Delta(0)/2\sqrt{2}\mu_B=1.83T_C$, for Ru_7B_3 with T_C 3.3 K,

yielding $H_p(0) \approx 6$ T. In our experiment the upper bound of H_{C2} ($99\%\rho_n$) is found to be about 5 T; the experimental value is obvious below Pauli limit, indicating that H_{C2} is still determined by orbital depairing fields. Another criterion is the presence of line or point node in the superconducting gap. The good fitting of specific-heat data with isotropic *s* wave has provided a strong evidence that Cooper pairs with spin singlet pairing symmetry dominates the superconducting condensate. The lower-critical-field measurement also gives the same conclusion even though the lower-temperature data (less than 1.2 K) are unfortunately absent. Thus a safe conclusion could be given that noncentrosymmetric superconductor Ru_7B_3 is dominated by *s*-wave pairing symmetry. While a further question is that why unconventional paring symmetry is absent or less populated in the present ruthenium-based noncentrosymmetric superconductor. From materials point of view, one simple explanation is that the mass of ruthenium is not heavy enough to induce a strong strength of spin-orbit coupling. A similar example is the noncentrosymmetric superconductor Li_2Pd_3B which is found to have a full gap, while Li_2Pt_3B has been proven to be a superconductor with line nodes.[10] Another possible explanation for the absence of unconventional pairing symmetry in Ru_7B_3 is the less extent of noncentrosymmetry. Referring to the structure illustration [Fig. 1(a)], the structure is observed to be symmetric from *ab* projection. From our band dispersion calculation, it is found that the splitting energy (ΔE) of bands cross the chemical potential is about 20 meV (except for some *k* points near Γ point for inadequate optimized initialization during computation); thus $\Delta E/k_BT_C$ of Ru_7B_3 is about 70, such a value is far below than that of noncentrosymmetric superconductors $CePt_3Si$ (Ref. 33) and Li_2Pt_3B (Ref. 34) ($\Delta E/k_BT_C > 1000$), but similar with that of Li_2Pd_3B and La_2C_3,[34,35] which belong to *s*-wave superconductor. Therefore the ASOC induced by noncentrosymmetry is not significant in Ru_7B_3.

After knowing the fact that the dominant pairing symmetry of Ru_7B_3 is *s* wave, a detailed investigation on the superconducting parameters is obviously worthwhile. Thus in the following discussion we will give a self-consistent calculation on the superconducting parameters of Ru_7B_3. In the measurement of magnetoresistance, the Kohler's rule was found to be only slightly violated, suggesting a symmetric Fermi-surface topology. Thus we could deduce the Fermi-wave number (k_F) from charge-carrier density (n),[36] assuming a single spherical Fermi surface, $k_F=(3\pi^2 n)^{1/3}=6.6527$ nm^{-1}, where $n=0.995\times10^{22}$ cm^{-3}. The effective mass is estimated as $m^*=(3\hbar^2\gamma_n)/(V_{\rm mol}k_B^2k_F)=17\ m_{\rm el}$, where $m_{\rm el}$ is bare electron mass and molar volume $V_{\rm mol}=136.89$ cm^3/mol. Then the Fermi velocity $\nu_F=\hbar k_F/m^*$ is about 0.47×10^5 m/s. The mean-free path is evaluated as $l=\hbar k_F/(\rho_0 ne^2)=31.36$ nm. In the clean limit the superconducting penetration depth equals to the London penetration depth; thus $\lambda_0=\lambda(0)=\sqrt{m^*/\mu_0 ne^2}$ is 214 nm. So the coherence length could be estimated using the BCS expression $\xi(0)=0.18\hbar\nu_F/(k_BT_C)$ as 19.5 nm.[30] Thus the above superconducting parameters could give a stringent checking on experimental data, such as $\xi(0)$ and H_{C1} and $\mu_0H_C(0)$. In the upper-critical-fields measurement, $H_{C2}(0)$ is determined as 1.1 T, so using $\xi(0)=\sqrt{\phi_0/[2\pi H_{C2}(0)]}$, where ϕ_0 is flux quanta, coherence length is 17.3 nm, such a value is very close to the deduced $\xi(0)$ 19.5 nm. For checking on H_{C1}, the following formula is used:[20]

$$\mu_0 H_{C1}=\left(\frac{\phi_0}{4\pi\lambda_0^2}\right)\ln\left(\frac{\lambda_0}{\xi_0}\right), \tag{7}$$

yielding $\mu_0H_{C1}=90.2$ Oe, where λ_0 and ξ_0 are deduced values from charge-carrier density. In our lower-critical-field measurement we obtain $\mu_0H_{C1}=110$ Oe, which is larger than the estimated value 90.2 Oe. The thermodynamic critical field $\mu_0H_C(0)$ could be obtained from the following formula:[20]

$$H_{C1}H_{C2}=H_C^2(0)\ln\left(\frac{\lambda_0}{\xi_0}\right), \tag{8}$$

using $H_{C2}=11000$ Oe, $H_{C1}=90.2$ Oe, $\lambda_0=214$ nm, $\xi_0=17.3$ nm, and $\mu_0H_C(0)$ is given as 628 Oe, which is very close to the value of 612 Oe determined by specific heat. For further checking on the experimental value of $H_{C1}(0)$, first by taking the experimental values H_{C1} (110 0e) and $\xi(0)$ (17.3 nm) into Eq. (7), one obtains $\lambda_0=189.3$ nm, then using this value $H_C(0)$ could be estimated by Eq. (8), yielding $H_C(0)=711$ Oe, which is about 100 Oe larger than that obtained from specific-heat measurement. Therefore it is safe to conclude that the intrinsic value of $H_{C1}(0)$ is about 90 Oe. In Table II we list the superconducting and normal-state parameters of the noncentrosymmetric material Ru_7B_3. Future efforts are strongly desired to clarify the origin of the onset transition on the resistive curve.

TABLE II. Superconducting and normal-state properties of Ru_7B_3.

Parameters	Ru_7B_3
γ_n (mJ/mol K^2)	80.15
$N(0)$ (state/eV cell spin)	20.988
Δ (meV)	0.5
H_{C2} (Oe)	11000
H_{C1} (Oe)	90
ξ (nm)	17.3
λ (nm)	214
κ	12.4
$H_C(0)$ (Oe)	612 ~ 628
Δ/k_BT_C	1.80
Δ_c/γ_nT_C	1.31
β (mJ/mol K^4)	0.3735
Θ_D (K)	470.175
E_c (mJ/mol)	192 ~ 205
m^*	$17m_e$
n (cm^{-3})	1×10^{22}
l (nm)	31.36
ρ_n ($\mu\Omega\cdot$cm) (4 K)	9

VII. SUMMARY

By conducting multiple kinds of measurements, we have extensively investigated the physical properties of the noncentrosymmetric superconductor Ru_7B_3. It is found that the superfluid density is dominated by a component with a full gap instead of a nodal gap, as revealed by the specific-heat and lower-critical-field measurements. Combining with resistivity (ρ_{xx} and ρ_{xy}) and electronic band-structure calculation, superconducting and normal-state physical parameters were determined by a self-consistent analysis; it is found that Ru_7B_3 belongs to a single band superconductor with energy gap 0.5 meV and could be categorized into a type-II superconductor with weak electron-phonon coupling. Anomalous kink has been found on the resistive curves at moderate fields, possible reasons are given to explain this "kinky" feature. We leave the questions concerning the two-step resistive transition under magnetic fields and why the possible spin-triplet pairing has not been clearly observed in this noncentrosymmetric material to future studies.

ACKNOWLEDGMENTS

This work is supported by the National Science Foundation of China, the Ministry of Science and Technology of China (973 project under Grants No. 2006CB601000 and No. 2006CB921802), and the Knowledge Innovation Project of the Chinese Academy of Sciences (ITSNEM). The author thanks T. Xiang for helpful discussion and L. Tang for technical support on electronic structure calculations. Appreciation is also given to C. Dong for the help of structure analysis.

*hhwen@aphy.iphy.ac.cn

[1] G. R. Stewart, Z. Fisk, J. O. Willis, and J. L. Smith, Phys. Rev. Lett. **52**, 679 (1984).
[2] J. G. Bednorz and K. A. Muller, Z. Phys. B. **64**, 189 (1986).
[3] Andrew Peter Mackenzie and Yoshiteru Maeno, Rev. Mod. Phys. **75**, 657 (2003).
[4] Y. Kamihara, T. Watanabe, M. Hirano, and H. Hosono, J. Am. Chem. Soc. **130**, 3296 (2008).
[5] E. Bauer, G. Hilscher, H. Michor, Ch. Paul, E. W. Scheidt, A. Gribanov, Yu. Seropegin, H. Noël, M. Sigrist, and P. Rogl, Phys. Rev. Lett. **92**, 027003 (2004).
[6] A. M. Clogston, Phys. Rev. Lett. **9**, 266 (1962).
[7] M. Yogi, Y. Kitaoka, S. Hashimoto, T. Yasuda, R. Settai, T. D. Matsuda, Y. Haga, Y. Onuki, P. Rogl, and E. Bauer, Phys. Rev. Lett. **93**, 027003 (2004).
[8] I. Bonalde, W. Brämer-Escamilla, and E. Bauer, Phys. Rev. Lett. **94**, 207002 (2005).
[9] Manfred Sigrist, D. F. Agterberg, P. A. Frigeri, N. Hayashi, R. P. Kaur, A. Koga, I. Milat, K. Wakabayashi, and Y. Yanase, J. Magn. Magn. Mater. **310**, 536 (2007).
[10] H. Q. Yuan, D. F. Agterberg, N. Hayashi, P. Badica, D. Vandervelde, K. Togano, M. Sigrist, and M. B. Salamon, Phys. Rev. Lett. **97**, 017006 (2006).
[11] M. Nishiyama, Y. Inada and Guo-qing Zheng, Phys. Rev. Lett. **98**, 047002 (2007).
[12] J. P. Morniroli, H. Ayatti, K. M. Knowles, W. M. Stobbs, and M. Gantois, J. Less-Common Met. **155**, 215 (1989).
[13] B. T. Matthias, V. B. Compton, and E. Corenzwit, J. Phys. Chem. Solids **19**, 130 (1961).
[14] C. Dong, J. Appl. Crystallogr. **32**, 838 (1999).
[15] S. Y. Savrasov, Phys. Rev. B **54**, 16470 (1996).
[16] B. Aronsson, Acta Chem. Scand. (1947-1973) **13**, 109 (1959).
[17] T. Masui, S. Lee, and S. Tajima, Physica C **383**, 299 (2003).
[18] M. Eisterer, M. Zehetmayer, and H. W. Weber, Phys. Rev. Lett. **90**, 247002 (2003).
[19] F. Bouquet, R. A. Fisher, N. E. Phillips, D. G. Hinks, and J. D. Jorgensen, Phys. Rev. Lett. **87**, 047001 (2001).
[20] T. Klimczuk, F. Ronning, V. Sidorov, R. J. Cava, and J. D. Thompson, Phys. Rev. Lett. **99**, 257004 (2007).
[21] G. Mu, Y. Wang, L. Shan, and H. H. Wen, Phys. Rev. B **76**, 064527 (2007).
[22] X. Y. Zhu, H. Yang, L. Fang, G. Mu, and H. H. Wen, Supercond. Sci. Technol. **21**, 105001 (2008).
[23] Q. Li, B. T. Liu, Y. F. Hu, J. Chen, H. Gao, L. Shan, H. H. Wen, A. V. Pogrebnyakov, J. M. Redwing, and X. X. Xi, Phys. Rev. Lett. **96**, 167003 (2006).
[24] N. P. Ong, Z. Z. Wang, J. Clayhold, J. M. Tarascon, L. H. Greene, and W. R. McKinnon, Phys. Rev. B **35**, 8807 (1987).
[25] H. H. Wen, G. Mu, L. Fang, H. Yang, and X. Y. Zhu, EPL **82**, 17009 (2008).
[26] N. P. Ong, Phys. Rev. B **43**, 193 (1991).
[27] H. Takeya, M. El Massalami, S. Kasahara, and K. Hirata, Phys. Rev. B **76**, 104506 (2007).
[28] W. L. McMillan, Phys. Rev. **167**, 331 (1968).
[29] T. Takeuchi, M. Tsujinoc, T. Yasudac, S. Hashimotoc, R. Settaic, and Y. Onuki, J. Magn. Magn. Mater. **310**, 557 (2007).
[30] M. Tinkham, *Introduction to Superconductivity*, 2nd ed. (McGraw-Hill, New York, 1996), p. 93.
[31] O. K. Andersen, Phys. Rev. B **12**, 3060 (1975).
[32] B. Wiendlocha, J. Tobola, and S. Kaprzyk, arXiv:0704.1295 (unpublished).
[33] K. V. Samokhin, E. S. Zijlstra, and S. K. Bose, Phys. Rev. B **69**, 094514 (2004).
[34] K.-W. Lee and W. E. Pickett, Phys. Rev. B **72**, 174505 (2005).
[35] J. S. Kim, Wenhui Xie, R. K. Kremer, V. Babizhetskyy, O. Jepsen, A. Simon, K. S. Ahn, B. Raquet, H. Rakoto, J.-M. Broto, and B. Ouladdiaf, Phys. Rev. B **76**, 014516 (2007).
[36] M. Kriener, Y. Maeno, T. Oguchi, Z.-A. Ren, J. Kato, T. Muranaka, and J. Akimitsu, Phys. Rev. B **78**, 024517 (2008).